Investigation of Fracture in Porous Materials: A Phase-field Fracture Study Informed by ReaxFF

Bang He[a], Truong Vo[a], Pania Newell[a,*]

[a]*Department of Mechanical Engineering, University of Utah, Salt Lake City, UT, 84112*

Abstract

Microscopic features (e.g, pore shapes, sizes, and distribution) in porous material substantially affect the overall mechanical properties such as stiffness and strength. In turn, these material properties determine the macroscopic behaviors of fracture in the porous material. In certain cases, macroscopic properties can be derived from the porous skeleton and void ratio (i.e., porosity), but in many other cases, such derivation is a challenging task. This paper presents a numerical investigation of microporosity and micropore shapes effect on the macrofracture behavior in porous amorphous silica. For this study, we extend the recently-proposed combined molecular dynamic (MD) and phase-field (PF) fracture modeling approach by including different pore shapes in the atomistic domain. In the MD simulations, we adopt ReaxFF to evaluate the material properties, where four different micropore cases are considered. Based on the material properties derived from MD simulations, the macrofracture propagation of porous media is studied using hybrid PF simulation. In the characterization of the pore structure, the concept of pore ligament is proposed to relate the pore shape and the critical energy release rate. Two classical fracture problems were used to evaluate the effect of pore shape on the macrofracture behavior. The results of the case study show that although the micropore shapes change the macrofracture behaviors, these effects vary with the geometry and loading conditions of macroscopic boundary value problems. The case study also shows that the influence of micropore structure can be captured at the macroscopic level through the material properties derived from the MD simulations.

*Corresponding author

Email address: Pania.Newell@utah.edu (Pania Newell)

Highlights

- Combine molecular dynamic and phase-field fracture modeling is extended to investigate the effect of underlying microstructure on the macrofracture behavior.
- ReaxFF molecular dynamic simulation is used for material characterization at the atomistic level.
- Higher-order parameters such as micropore shapes affect macrofracture behavior.

Keywords: Multi-scale, Heterogeneous porous materials, Molecular dynamics simulations, Hybrid phase field, Fracture mechanics

1. Introduction

Porous media/materials widely exist in substances in nature (e.g., bone, rock, soil, etc.) and in man-made materials (e.g., concrete, ceramic, foams, etc). These substances consist of matrix and open or close pore spaces that exhibit many promising properties such as lightweight, excellent heat conductivity, high permeability, and desirable interaction between matrix surface with fluid/gas within the pores. Therefore, porous media have been appealing to a variety of engineering and scientific fields [46] from material sciences to geosciences as well as from biosciences to bioengineering, etc. [28].

Determining the mechanical properties of porous media is an essential aspect in predicting porous materials' response to different external loading conditions. Many studies have highlighted how material properties (e.g., stiffness, strength, permeability) of porous media are impacted by the underlying micropore structures [1] including pore shape, pore size, and pore network [49, 40, 81, 20, 65]. Also, the study [36] shows that the morphology of any porous media is completely deterministic so studying the relation between pore structure and the mechanical properties of porous media is feasible.

However, to the best of our knowledge, the effect of micropore structure (e.g., pore shape) on the macrofracture behavior in porous media has not been fully

[1] In this study, for convenience, from now, we refer to microscopic variables or quantities related to nano pores as micro or microscopic. For instance, micropore, microscale, microfracture, microscopic material properties, etc.

investigated [18]. Particularly, the pore shape effect is rarely quantified in the characterization of macroscopic mechanical behaviors. Therefore, in this study, we are interested to estimate the material properties as a function of underlying pore structures and investigate their effect on the macrofracture behaviors.

Even though for certain porous media, material properties can be characterized based on their micropore structure, it is often challenging to characterize properties such as elastic stiffness and fracture toughness of a heterogeneous porous media in terms of their microstructure [17, 22, 76, 66]. Recently, some researchers have investigated the impact of microstructure (pore size, pore distribution, and orientation) on the overall stiffness of porous media [89, 42, 79, 43, 90, 50, 44]. Vazic et al. [83] highlighted the role of pore structure on higher-order parameters even beyond the stiffness tensor. Other works established a relation between fracture toughness and micropore structure [44, 66, 20, 37, 33]. However, in these studies, the established relations are limited to certain types of pore structures or porous media [20, 15, 37], while many porous structures pose geometrical complexity. For instance, some porous structures are homogeneous but some are not, and some have complex hierarchical porous structures. Therefore, it is still a challenging task in the characterization of complex porous media.

In the past decades, molecular dynamic (MD) simulation has demonstrated significant accuracy in obtaining material properties, and have been widely used to establish various properties such as elastic stiffness, fracture toughness, etc. [93, 85, 25, 45, 12, 72, 84, 41, 21]. In the same fashion, MD is also a powerfully numerical tool to characterize porous materials [45, 84, 21]. Furthermore, considering that the variation of the pore sizes in some porous materials ranges from sub nanometer to hundreds of nanometers, MD is a great candidate to model such complex hierarchical structures.

Due to the close relevance to the industrial needs, fracture in porous media has been the central focus in many fields. In the past decade, with the significant advancement of numerical methods for modeling fracture behavior in porous materials, there has been an increasing amount of attention to investigate fracture mechanism in these complex systems [18, 33, 57, 94]. These methods include extended finite element method (XFEM) [4, 58, 7, 59, 29, 78, 2], isogeometric analysis [64, 9, 14], damage gradient method [19, 70], and phase-field (PF) fracture modeling [55, 56, 54, 34, 88, 51].

Because of the promising features of phase-field (PF) framework, PF has been adopted in a series of fracture investigations in porous media [56, 54, 34, 88, 86,

91, 94, 24, 77]. One such feature is the introduction of diffusive variables that is used to regularize the sharp crack zone to a diffusive zone based on Griffith's theory [27]. The crack propagates as the surface energy reaches a threshold value where the PF variable takes the value of one within the broken domain and it is zero in the unbroken domain, with smooth transition between these two regions. Using this method, fracture discontinuity can be avoided in numerical modeling. Furthermore, the fracture path does not need to be pre-defined with any special treatments in the discretization step.

In the PF framework for porous media, the fracture threshold value (usually critical energy release rate G_c), Young's modulus, and Poisson's ratio are required as the material properties. These properties are generally obtained from experiments [91, 56, 54, 11]. However, these experimental measurements are typically based on the macroscopic behavior while the variation of micropore structures is usually ignored. Therefore, the pore structure effect is difficult to be captured in such experimental measurements. Some recent studies [33, 5] propose to use numerical homogenization to obtain material elastic properties for PF fracture modeling in porous media so that the effect of the micropore can be considered. However, the effect of micropores on critical energy release rate is not considered in these works.

To account for the multiscale nature within PF fracture modeling, several papers proposed to use combined MD and PF technique [30, 68, 67]. The basic idea is to derive the material properties from MD simulation and subsequently implement them in the PF fracture model. Due to the promising feature of this multi-scale approach, we adopt similar method in this study. However, we use reactive force field (ReaxFF) for the first time in MD-informed PF modeling. We also explicitly model different pore structures at the atomistic level. Furthermore, in those studies, the framework was limited to simple fracture models (e.g., single (double) edge plate under tension) with comparable size in microscale and macroscales, but we extend this framework by reforming the critical length scale from the MD-based material properties so that the extended PF-MD framework can be applied to complex fracture problems at the macroscale, which may not be available by using either compuatational intesive MD or literature-proposed approaches [30, 68, 67]. It should be noted that amorphous silica is a common material in many engineering application and thus our study focuses on amorphous silica. However, this framework is applicable to other porous materials as well.

The rest of the paper is organized as follows. The PF fracture technique, ReaxFF MD, and combined MD and PF modeling approach are introduced in the second, third, and fourth sections, respectively. The evaluation of MD simulation associ-

ated with derived material properties is presented in the fifth section. In the sixth section, two fracture models are used to analyze the pore morphology. Finally, we will wrap up with the conclusion sections.

2. Phase-field fracture modeling

2.1. Brief introduction of phase field fracture modeling

Phase-field fracture modeling is a promising method to study macro fracture behaviors, which has been extensively developed for brittle and ductile fracture [53, 61, 33, 95, 6, 57, 35, 1, 48, 47]. A comprehensive review can be found in [87]. The essential idea in PF is to use a diffusive phase-field variable, ϕ, to regularize the sharp crack that equals to zero if the material is unbroken and equal to one if it is totally broken (physically, the crack is not a discrete phenomenon and crack width is approximately zero) [19]:

$$\phi(\mathbf{x},t):\begin{cases} 1 \ \text{ as } x=0 \\ 0 \quad \text{as} \quad x\rightarrow\pm\infty \end{cases}, \tag{1}$$

where the length parameter, l_0 controls the size of the diffusive area.

The concept of the diffusive zone is shown in Figure 1, where the red region is the diffusive zone defined by the phase-field variable.

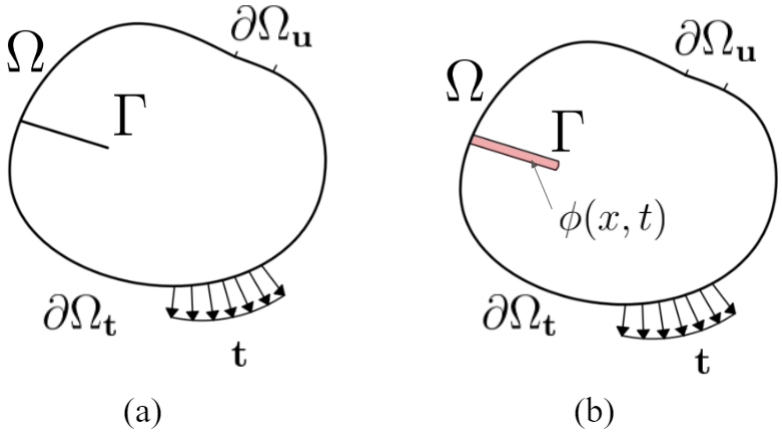

Figure 1: Schematic of (a) sharp crack, (b) diffusive zone of crack [32].

In the PF framework, the potential energy in a fractured solid body is equal to the sum of the bulk energy $\psi_{\mathbf{u}}$ associated with the unbroken solids and dissipated fracture energy ψ_ϕ during the fracture propagation:

$$\psi = \psi_{\mathbf{u}} + \psi_\phi. \tag{2}$$

There exist a couple of different theories explaining the fracture propagation driving force in the PF framework. The detailed discussion of fracture evolution theory is available in the literature [8, 3, 87]. In this study, we use so called AT2 fracture model [63], where the strain energy is split into compressive and tensile energy, and the crack propagation is driven by tensile strain energy, as illustrated in Equation 3 [51],

$$\begin{aligned} \operatorname{div}(\boldsymbol{\sigma}) + \mathbf{b} &= 0, \\ G_c \left(\tfrac{1}{l_0}\phi - l_0 \Delta\phi \right) - 2(1-\phi)\psi_0^+(\boldsymbol{\varepsilon}) &= 0, \\ \boldsymbol{\sigma} \cdot \mathbf{n} &= \mathbf{t} \ on \ \partial\Omega_t, \\ \nabla\phi \cdot \mathbf{n} &= 0 \ on \ \partial\Omega, \end{aligned} \tag{3}$$

where $\boldsymbol{\sigma}$, $\boldsymbol{\varepsilon}$, $\mathbf{b}$, and $\mathbf{t}$ are the Cauchy stress, strain tensor, volume forces applied to the solid, and traction, respectively. G_c is the critical energy release rate; ψ_0^+ is the positive elastic energy [53]; and l_0 is the critical length scale; Δ is the Laplace operator; ∇ is the gradient operator. Neumann-type boundary $\partial\Omega_t$, and Dirichlet-type boundary $\partial\Omega_u$ are also shown in Figure 1, and $\mathbf{n}$ is the normal vector on the boundary. It should be noted that in our case studies, the volume force is not considered.

It should be noted that splitting the strain energy leads to an anisotropicity in the PF governing equation (Equation 3), where the stiffness only degrades in the direction orthogonal to the crack. Therefore, the load in the other direction can still be sustained by the fully broken region [38]. In this study, considering the computational cost and accurate stiffness degradation for complex loads, the hybrid formulations of the PF framework are used.

2.2. Hybrid formulations of phase-field fracture modeling

The hybrid formulation of the PF fracture modeling was initially proposed by Ambati, et al. [3]. In this framework, the strain energy is updated by the linear momentum equation (Equation 4a), and the fracture propagation is driven by the positive strain energy (Equation 4b). To avoid the interpenetration of fracture under compression load, a constraint described in Equation 4c is imposed to the

system. Thus the anisotropic formulations read:

$$\begin{cases} \boldsymbol{\sigma}(\mathbf{u},\phi) = (1-\phi)^2 \dfrac{\partial(\psi_0(\boldsymbol{\varepsilon}))}{\partial \boldsymbol{\varepsilon}}, & \text{(4a)} \\ -l_0^2 \Delta\phi + \phi = \dfrac{2l_0}{G_c}(1-\phi)H^+, & \text{(4b)} \\ \forall \mathbf{x} : \psi_0^+ < \psi_0^- \rightarrow \phi \equiv 0. & \text{(4c)} \end{cases}$$

where H^+ is a history variable defined to prevent the reversibility issue of fracture, Δ is the Laplace operator, and $\mathbf{u}$ is the displacement vector.

Compared to the classical anisotropic PF formulation [55], the hybrid form avoids the unrealistic fracture pattern under mixed tension and compression cases, in which anisotropic formulation only degrade the stiffness orthogonal to the crack. Another benefit from the hybrid form is its lower computation cost as it avoids the unsymmetrical stiffness in the finite element implementation [3, 38, 87]. The study by Ambati, et al. [3] showed how the hybrid approach is several times faster than the classical anisotropic method.

2.3. Verification of numerical implementation

Considering the above advantage of hybrid formulation, in this study, we adopted and implemented it in our research code. To verify the correct implementation of the hybrid formulation, we used two fracture models: the single-edge notched shear model reported in [23] as shown in Figure 2, and notched rectangular specimen with three openings reported in [61] and shown in Figure 5.

2.3.1. Single edge-notched shear model

The single edge-notched shear model is widely used to verify the PF fracture results by many researchers [53, 23, 60, 61]. The dimension of the plate is 1×1 mm^2 with a pre-existing crack located in the middle of the left edge as shown in Figure 2. The crack is 0.5 mm long and the bottom edge of the square is fixed while a displacement load is applied to the top edge.

To illustrate the mesh convergence, the area right behind the preexisting crack in the model is discretized with three different meshes size, h=0.0035 mm, 0.0017 mm, and 0.0011 mm. They have 16560, 24630, and 37582 quadrilateral elements respectively. A prescribed displacement is applied with a 0.00001 mm increment that is the same as the reference model reported in [23]. Material properties used in this study are the same as [23], specifically, these parameters are: Young's modulus, E=210 GPa, Poisson ratio ν=0.3, critical energy release rate G_c=0.0027 KN/mm, and critical length scale L_0=0.0075 mm. The reaction force of three

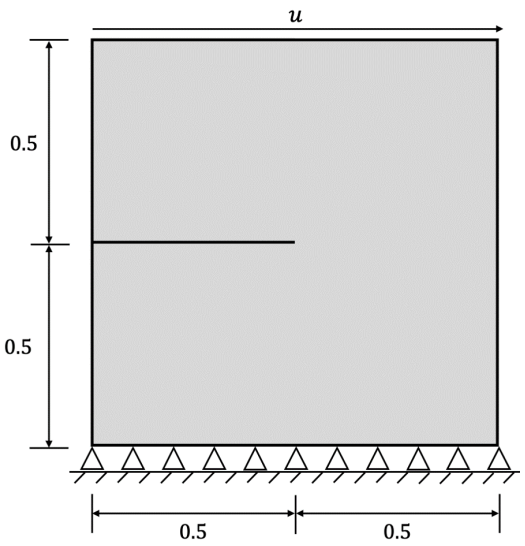

Figure 2: Schematic of single edge notched fracture model.

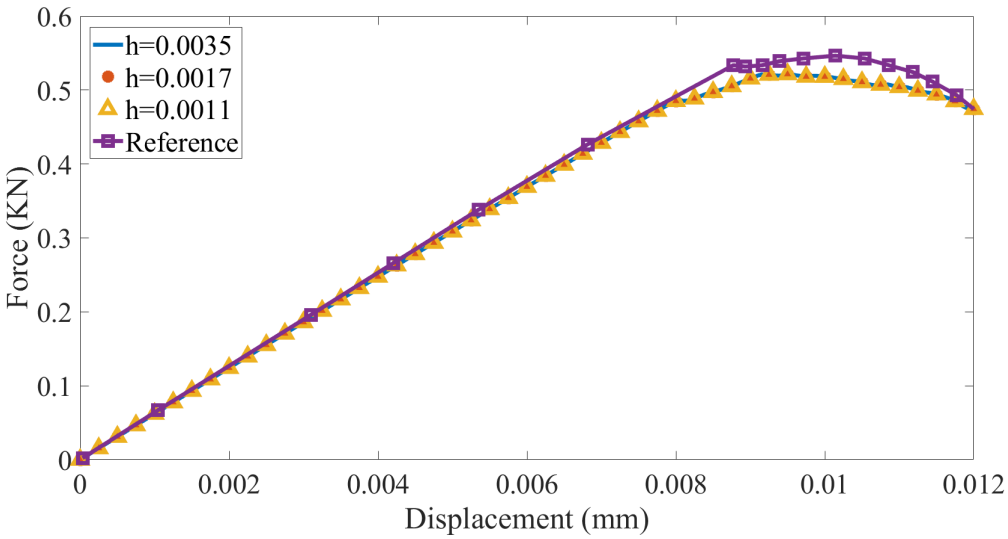

Figure 3: Reaction force plot of three different meshes.

models are plotted in Figure 3 while Figure 4 shows the fracture path in the reference model and our newly-implemented model.

From Figure 3, one can see that the force-displacement associated with all three different meshes are almost identical. This indicates that sufficiently small size meshes were selected in all these cases and thus guarantee that the converged

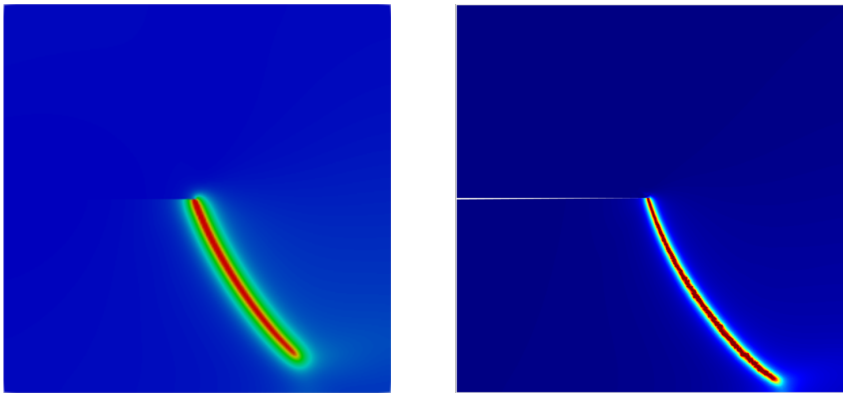

Figure 4: Comparison of (a) reference fracture path [23], (b) fracture path in our simulation (h=0.0017 mm).

solutions were obtained. Also, the max reaction force is similar to the reference result as illustrated in Figure 3, where the reference plot is digitized from Figure 18 in [23] (The small discrepancy can be attributed to the different discretization between reference model and our model.). Moreover, Figure 4 (b) shows the fracture paths obtained from our simulation is quite comparable with the fracture path reported in 4 (a).

2.3.2. Notched rectangular specimen with three openings

The tensile test for a notched rectangular specimen with three openings was introduced by Msekh et al. [61]. In this model, a notch is located at the left edge of the plate and three holes are horizontally placed at 20 mm above the notch. The bottom of the plate is fixed and a pull-up displacement is applied to the top edge. The dimension of the plate is 150×200 mm^2. The three holes are 40 mm apart. The schematic of this fracture problem is illustrated in Figure 5. The model is discretized by 13,960 quadrilateral elements with an average element size of 0.2 mm.

The prescribed tensile displacement at the top of the domain is 0.45 mm and the increment load is 0.0004 mm (the increment size is not specified in the reference model). Since the increment size affects the simulation result, we performed sensitivity analysis and selected the increment size of 0.0004 mm as the optimal value where the fracture pattern is no longer influenced by smaller increment sizes. The total number of increments in each simulation is 1,500 increments. In reference [61], the material properties used for this model is not detailed. In our model, we use Young's modulus E=18 GPa, Poisson's ratio ν=0.2, critical energy release

rate G_c=0.002 KN/mm, and critical length scale L_0=0.1 mm. The fracture path is illustrated in Figure 6 (b).

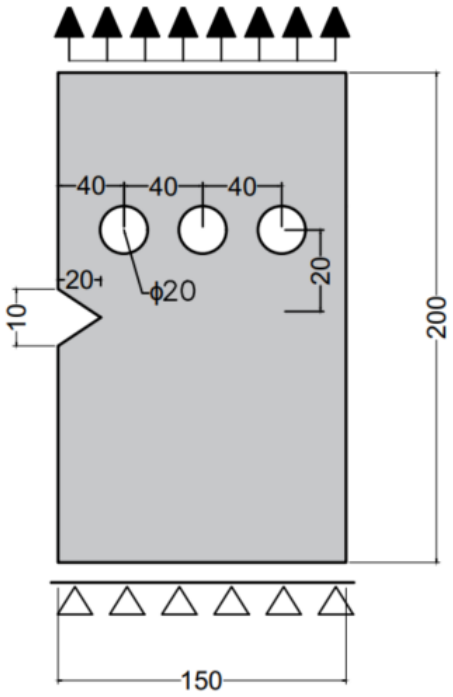

Figure 5: Schematic of notched rectangular specimen with three openings.

Comparing Figure 6 (a) and (b), one can see the fracture path in our simulation is quite similar to the fracture path in the reference model while the some small differences is observed. For example, the initial crack path is straight in Figure 6 (b) but slightly curved in Figure 6 (a). Also, the penetration location of fracture in the middle circle edge is different. These discrepancy might be due to the difference in material properties and increment size.

However, the similar fracture paths in these two models indicates that we have properly implemented the hybrid formulation introduced above. Therefore, we will use the verified hybrid formulation to study the underlying micropore shape effect on the macrofracture behavior of porous media. Specifically, above single edge-notched shear model and notched rectangular specimen with three openings model will be reused as case study in section 6.

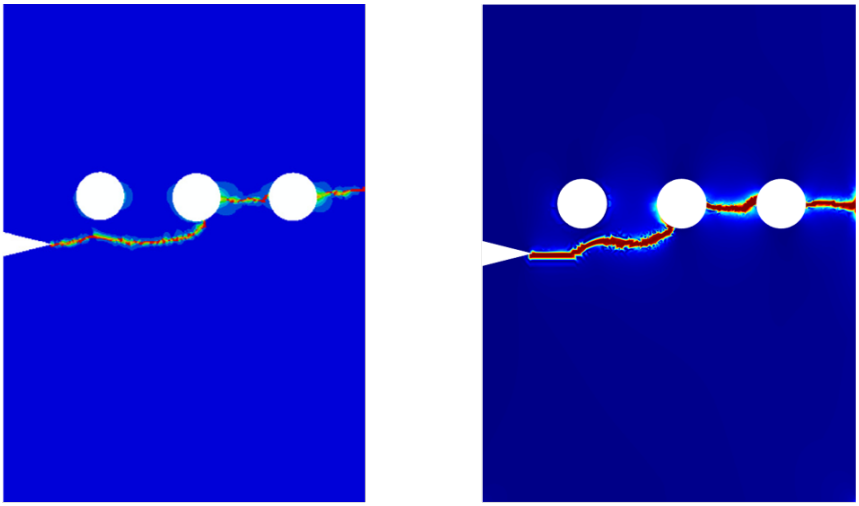

Figure 6: (a) reference fracture path [61], (b) fracture path in our simulation.

3. ReaxFF MD simulation and material properties characterization

Molecular dynamic simulation solves Newton's equations of motion for a set of interacting particles at the atomic scale. The interactions among particles are governed by an interatomic potential. Therefore, by using MD simulation, we could derive some important material properties (e.g., energy release rate) that are impossible in other numerical approaches [33]. However, one challenge in MD simulations is the selection of an appropriate force field that can be extended to different compositions. This limitation exists in some classical MD force fields, e.g. Beest-Kramer-van Staten (BKS) [82], Tersoff [62], Stillinger-Weber (SW) [75], and Pedone [69], which have been discussed by Rimsza et al. [73]. For instance, in these methods, force fields are rarely designed to simulate high strain conditions and do not represent varying compositions to identify the role of network modifiers and formers on crack growth. These limitations become critical when modeling fracture dynamics of silica glass [73], which is the base material used in this study.

3.1. Reactive force field molecular dynamics (ReaxFF)

To overcome the above-mentioned challenges, the state-of-the-art reactive force field (ReaxFF) is proposed [82]. ReaxFF is a reactive bond-order based force field and usually derived by fitting against a training set comprising both quantum mechanics and experimental data. In Reaxff, the total energy of the system includes

ten energy terms as:

$$E_{\text{total}} = E_{\text{bond}} + E_{\text{over}} + E_{\text{under}} + E_{\text{lp}} + E_{\text{val}} + E_{\text{pen}} + E_{\text{tors}} + E_{\text{conj}} + E_{\text{vdW}} + E_{\text{coul}}. \quad (5)$$

E_{bond} is a term describing the energy of single, double, and triple bonds, E_{over} and E_{under} represent the energy terms of complex interactions, which cause a specific atom type to have over and under coordination with other atom types, respectively. E_{lp} is the energy term modeling the lone electron pairs, E_{val} is the energy term related to the valence angle, which is created by over/under the coordination and lone electron pair energy term. E_{pen} is an additional energy term that takes into account the penalty coming from the cumulative double bonds in a particular valency angle. E_{tors} is the energy term that describes all different torsional configurations, E_{conj} is the energy contribution representing the conjugated double bonds effect. E_{vdW} is the energy term accounting for non-bonded interactions and E_{coul} is the energy contribution due to the electrostatic interactions.

In this study, MD simulations are carried out using LAMMPS, an open-source code developed at Sandia National Laboratories [71]. The time step was set to 0.25 fs, which is similar to other studies [31, 52]. All the interaction and reaction parameters in the amorphous silica (a-SiO_2) model were obtained from literature [26].

3.2. MD-based material properties characterization

The MD-based material characterization is a critical step in combined molecular dynamics and PF fracture modeling. Two scales are linked by deriving four material properties (i.e., Young's modulus E, Poisson's ratio ν, and critical strain energy release rate G_{C}) from the MD simulations, and subsequently using these MD-based material properties to construct the fracture behaviors modeled by PF fracture technique. The approach for deriving these material parameters is briefly discussed below. For the detailed discussion, readers are referred to our previous work by Vo et al. [84].

Young's modulus E is determined from the slope of the initial linear region (up tp 5% strain) of the stress-strain curve, where stress is calculated using virial stress as presented in [80].

$$\sigma_{kl} = -\frac{1}{V}\left(\sum_{i}^{N} m_i \mathbf{u}_{ik} \otimes \mathbf{u}_{il} + \frac{1}{2}\sum_{i}^{N}\sum_{j\neq i}^{N_c} \mathbf{r}_{ijk} \otimes \mathbf{F}_{ijl}\right). \quad (6)$$

The first and second terms on the right-hand side of Equation 6 denote the kinetic and virial contributions, respectively. k and l are the components regarding the

Cartesian coordinate system, m_i is the mass of the particle i, $\mathbf{u}_{ik}$ and $\mathbf{u}_{il}$ are the velocity components of the particle i along with the directions k and l, respectively, where the bias velocity due to deformation is removed. N and N_c are the numbers of particles in the system and within the cutoff radius around particle i, respectively. The term $\mathbf{r}_{ijk}$ is the distance vector component along direction k between the two particles i and j, and $\mathbf{F}_{ijl}$ is the inter-molecular force exerted on particle i by particle j along the direction l. V is the volume of the system.

The Poisson's ratio, ν, is calculated as:

$$\nu = -\frac{d\varepsilon_y}{d\varepsilon_x}, \tag{7}$$

where $d\varepsilon_y$ and $d\varepsilon_x$ are the strain in the y- and x-directions, respectively. The calculation of critical energy release rate, G_{IC}, is based on the approach proposed by Brochard et al [10], where G_{IC} is the stored mechanical energy released upon crack is formed. The equation read:

$$G_{\mathrm{C}} = \frac{L_y L_z}{\Delta A} \int_{L_x}^{L_x^c} \sigma_{xx} dL_x, \tag{8}$$

where L_x indicates initial dimension of sample in X direction, as shown in Figure 9(b). L_x^c is the ultimate dimension when the sample is totally broken. L_y, and L_z are the dimension of sample in Y and Z respectively.σ_{xx} is the average stress at the left and right side of sample. ΔA is the total area of a newly created crack. While the focus of our study is on mode I fracture, according to Brochard et al [10], this method also applies to mode II fracture.

4. Combined MD and PF fracture modeling approach

The combined MD-PF approach consists of two steps: 1) deriving the material properties from MD simulations of the molecular systems and 2) replacing the corresponding parameters in the macrofracture simulation using the PF framework. The potential of this multi-scale fracture modeling approach has been previously demonstrated in the works by Hansen-Dörr et al., [30], Patil, et al. [68, 67], and Satake, et al. [74].

In this multi-scale framework, the material properties obtained from the discrete atomic simulations capture the physics of the material closely and the measured MD-based parameters are more accurate comparing to the empirical values. Moreover, this approach enables us to look into the intrinsic defects or microaspects from the atomistic scale. In the PF fracture modeling, material parameters are informed by the material properties obtained from the MD simulations, and as

a result, the microscopic structural effect on the overall fracture behavior of the material will be considered. Thus, we believe, the MD-informed PF modeling approach is a physics-driven method providing an effective way to link the microstructures variations to the fracture behavior in the continuum scale [68]. In these studies, two comparable fracture models, the molecular dynamic model, and this cross-scale PF fracture model show a good agreement in terms of fracture pattern, reaction force, energy dissipation, etc.

Inspired by the existing MD-PF works available in the literature, we extended this two-scale modeling framework to a more general form, where the MD and PF models are not necessary to be the same model in the same length scales. In the MD simulations, the fracture models are in a microscale subject to simple tensile loading (i.e., mode I fracture), while PF models are in macroscale and subject to complex loading scenarios (e.g., combined tension and compression loads, etc.), which may be a challenging work in MD modeling.

Furthermore, in obtaining material properties via MD simulations, we adopt the state-of-the-art ReaxFF that has been proven to be able to predict the material mechanical properties more accurately than other force fields [82]. In MD models with ReaxFF, we introduce micropores to capture the influence of pore shape in measured material properties [84] and subsequently in PF fracture modeling.

With this extension, we can investigate fracture models that have complex geometries and may not be possible in MD modeling. However, this extension requires reforming the critical length scale in PF to remediate the scale difference, because the methods of estimating length scale proposed in literature [30, 68] is not applicable to fracture models with complex geometries as discussed in section 6.3. To resolve this issue, we adopt the macroscopic material properties-based approach proposed by Zhang et al. [92].

5. Material properties characterization of a-SiO_2 samples

As mentioned above, this study focuses on a-SiO_2 as the material of choice. The details of the material characterization are presented below.

5.1. Material development and tensile loading models

In the MD simulations, a-SiO_2 was created through a melt-and-quench procedure starting with a simulation box of $4.95\times4.95\times1.53$ nm^3 of β-cristobalite. A detailed description of the sample development processes was presented in our previous study [84]. The comparison of the final structure of a-SiO_2 with the experimental data shows an excellent agreement. Therefore, we believe that our a-SiO_2 model

can be used for further investigation of the shape effect of micropore on macrofracture behaviors.

In this MD model, the tensile loads are applied to two opposite sides of the a-SiO_2 sample as illustrated in Figure 9b. Four different sample models are created: (1) without a pore, (2) with a circular pore, (3) with a triangular pore, and (4) with a square pore, as shown in Figure 7. Each pore is located at the center of the simulation box. The dimensions of all models are 29.41× 29.41×1.51 nm^3, which was made by replicating a 6×6×1 nm^3 sample in all three directions [84]. The size of each pore was decided based on 2.27% porosity which remains constant for all cases regardless of the pore shape. A strain-controlled periodic boundary conditions were applied to the sample as shown in Figure 7a and the tensile displacement is applied in the x-direction with a strain rate of 8×10^9 s^{-1}. This strain rate is within the linear regime [13], where Young's modulus from the MD simulations is in good agreement with experimental data. Moreover, other researchers Vo et al. [84], Chowdhury et al. [13**?**] NPT ensemble was used to control the temperature and pressure of the system at 300 K and 1 atm, respectively.

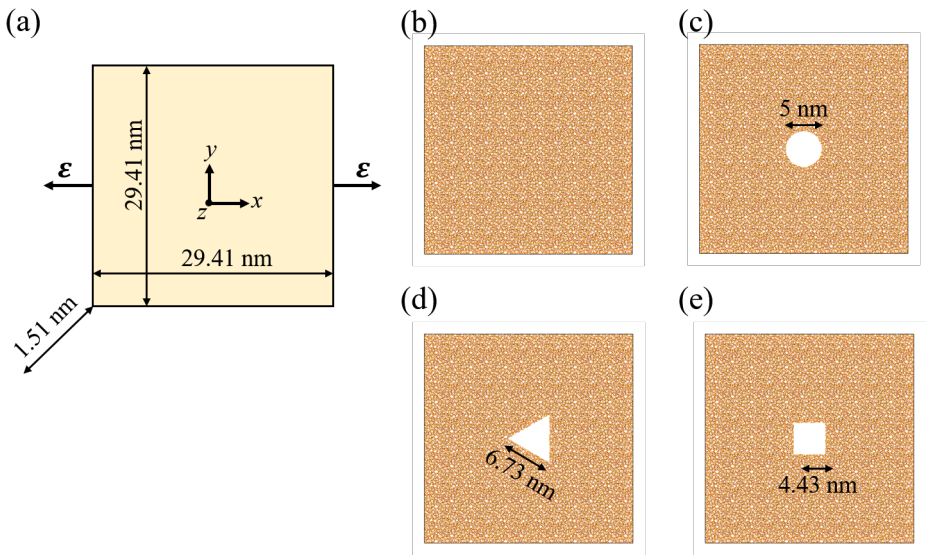

Figure 7: (a) Schematic diagram of a MD simulation of tensile loading of a-SiO_2. (b)-(e) Four MD samples will be employed in this study. Specifically, a bulk a-SiO_2 (b) without any void, (c) with a circle pore, (d) with a triangle pore, and (e) with a square pore.

The major parameters including the sample size, particle amount, and microporosity for each sample are summarized in Table 1. Among the four micro models, the case without micropore (i.e., zero porosity) is used as the reference case.

Table 1: Dimensions, number of atoms, and porosity of MD models applied in this study.

MD model	**Without pore**	**Circular pore**	**Triangular pore**	**Square pore**
Dimension (nm^3)	29.41×29.41×1.51	29.41×29.41×1.51	29.41×29.41×1.51	29.41×29.41×1.51
Number of atoms	86,400	84,462	84,442	84,462
Porosity (%)	NA	2.27	2.27	2.27
Pore ligament (nm)	NA	12.50	11.64	12.79

From the molecular simulations of these four microscopic models, Young's modulus E, Poisson's ratio ν, and energy release rate G_c are directly calculated according to the approaches described in Section 3.2. The crack diffusive length L_0 for PF fracture modeling is calculated indirectly, and critical stress is obtained from the available literature.

5.2. Derivation of material properties based on MD simulations

The method of evaluating Young's modulus, Poisson's ratio, and the critical energy release rate has been introduced in Section 3.2. In the following, the approach to calculating the length scale is carefully discussed.

The critical length scale is an important parameter in the PF fracture modeling and it was evaluated differently in the work published by Patil et al. [68, 67] and Hasnsen-Dorr et al. [30]. In the former, the length scale is calculated as a function of density concentration that correlates with the crack transition zone in the MD simulation. In the latter, an arbitrary value in the same order as the distance between the atoms is selected to conduct the PF simulation. They also proposed to initially estimate a length scale using a method proposed in [92] and continuously correct it based on the MD results. A common limitation for these two approaches is that the MD model and PF model need to have comparable geometry and loading conditions. This imposes a restriction on combining the MD and PF frameworks. In our study, since the crack phase transition in MD has been upgraded to the macrolevel by energy release rate, we postulate that the MD-based macroscopic material properties considered the scale difference. Therefore, the critical length scale can be estimated from the macroscopic material properties based on Equation 9 proposed in [92]:

$$L_0 = \frac{27EG_c}{256\sigma_{cr}^2} \tag{9}$$

where L_0 is the critical length scale, E is Young's modulus, G_c is the critical energy release rate, and σ_{cr} is the critical tensile strength. From the macroscopic point of view, Equation 9 reveals the connection of critical length scale with material properties so it provides an approach to properly estimate the critical length scale

without knowing the nano transition zone.

As one can see from Equation 9, the critical tensile strength is needed. In this study, the characterization of material properties is based on the mode I fracture of microsamples subjected to the tensile load so the critical tensile strength can be estimated based on the MD simulations. However, as discussed in [12], the critical tensile strength estimated based on an MD simulation is much higher than the theoretical limits as well as experimental value at the continuum scale. This overestimation is caused by the high-strain rate of loading in the MD simulation and ignore the role of defects at macrolevel. To properly calculate L_0, we obtain the tensile strength of a sample without micropore based on the available data in the literature [39]. This value will be modified for the samples with pores according to the ratio of their ultimate strain value to the ultimate strain of the sample without pores.

Based on the above-mentioned approaches, the material properties of each microscopic sample are derived and summarized in Table 2. In the next section, these material properties will be applied to the PF fracture models to study how micropore structure affects macrofracture behaviors of a-SiO_2 plates.

Table 2: The mechanical properties including Young's modulus E, Poisson's ratio ν, and critical energy release rate G_{IC}) that were obtained from MD simulations.

MD model	**Without pore**	**Circular pore**	**Triangular pore**	**Square pore**
E (GPa)	72.83	68.23	66.45	67.76
ν	0.34	0.37	0.38	0.37
G_{c} (J/m^2)	17.41	12.57	10.13	12.75
σ_{cr} (MPa)	150.00	89.35	71.26	104.86
Ł$_0$ (10^{-3}m)	0.06×10^{-1}	0.11×10^{-1}	0.14×10^{-1}	0.08×10^{-1}

5.3. Energy release rate and microporous structure

In porous media, the porosity is an important quantity in characterizing the stiffness of the media, as a large number of studies show their close relationship [15, 33, 37, 20]. Our MD-based material characterization reveals a similar trend as illustrated in Table 2. Specifically, the introduction of a porosity value of 2.27% leads to lower estimated Young's modulus values compared with a case with zero porosity (i.e., 72.83 GPa). This drop in Young's modulus value is independent of the pore shape and the average Young's modulus for all these cases is 7% lower than the case without pore. However, a closer look at Young's modulus values reported in Table 2 shows that the pore shape has an influence on Young's modulus.

To the best of our knowledge, the effect of pore shape on the fracture is still not fully investigated. Even though there exists some research discussing the pore size and distribution impact [37, 79, 43, 16, 20], there is no work which discusses the role of pore from the atomic scale onto continuum scale. However, our recent study [84] illustrated that the material properties at the atomic scale vary along with the change in the pore shape, where we have used the concept of ligament length to correlate the pore shapes and the energy release rate for cases with single pore. Here, we discuss this concept in more detail as we are building our new upscaling approach.

In our molecular dynamics simulations, we primarily focus on porous materials with a single closed pore with periodic boundary conditions subject to tensile loading, where the middle section experiences the largest strain. Therefore, the crack usually initiates from the centerline of the sample perpendicular to the loading direction as illustrated in Figure 8. As one can see from this figure, the crack propagation patterns are similar for all cases, since each pore is positioned at the center of the simulation box.

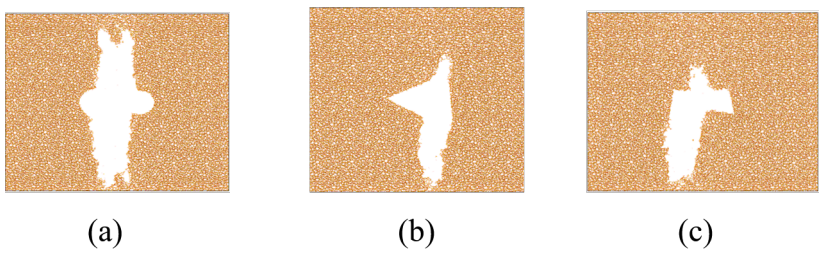

Figure 8: Example of crack propagation pattern for the cases with (a) circular pore, (b) triangular pore, and (c) square pore.

The evaluation of the energy release rate is based on the fracture surface as discussed in Equation 8, where the energy release rate is the integral of strain energy along the fracture surface, from L_x to L_x^c. Therefore, accurate measurement of the fracture surface (shown in Figure 9) in the MD simulation is critical for the dissipated energy during fracture propagation.

Since each case has the same thickness, the distance from the pore boundary to the edge of the simulation box is closely related to the G_c value. Roughly speaking, a longer distance results in a higher release of fracture energy, which means higher G_c. However, in complex pore geometries such as the oval, circular, triangular, and/or any irregular pore shapes, the distance from the pore boundary to the edge of the simulation box is not usually uniform. To universally quantify the impact of

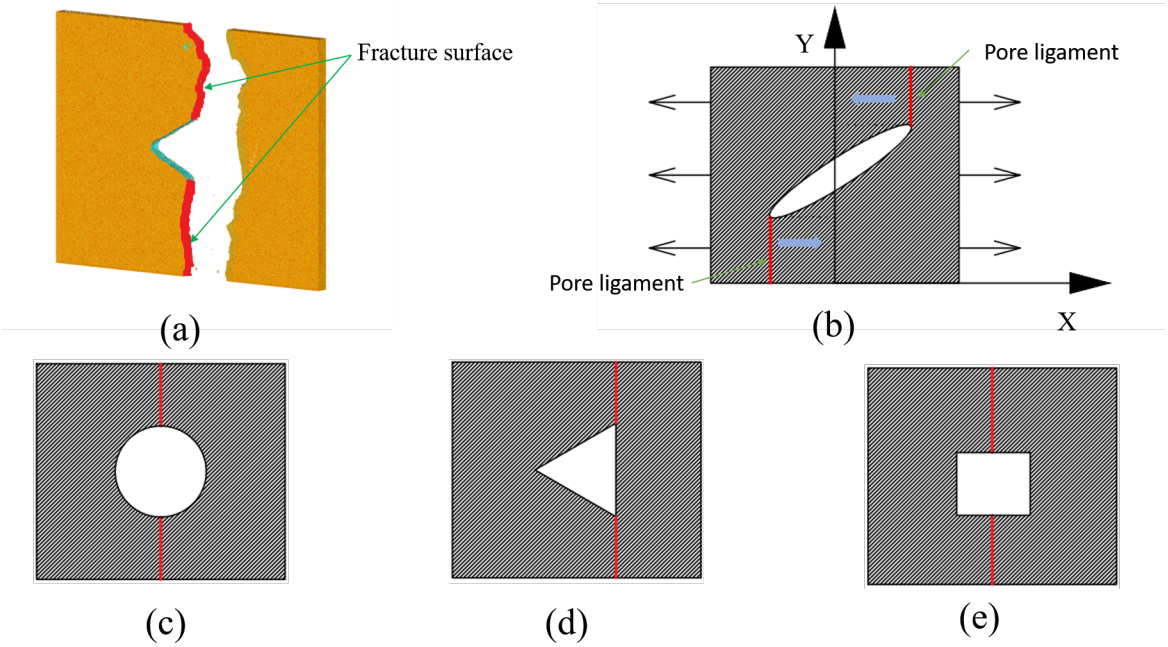

Figure 9: Schematic of (a) fracture surface, (b) loading condition and pore ligament, (c) ligament of circular pore, (d) ligament of triangular pore, (e) ligament of square pore.

this distance, a projection or ligament length defined as the shortest length from the pore boundary to the simulation boundary can be used. In Figures 9b,c, d, the red lines represent the ligament lengths for each case with a different pore shape. The ligament length of each case is listed in Table 1. Moreover, the energy release rates of each case obtained from the MD simulations are also listed in Table 2. From this table, one can see that the value of G_c increases with an increase in the ligament length.

6. ReaxFF-informed PF: Case studies

In this section, two classical fracture models from the verification study in section 2.3 are used to illustrate how the structure of micropore influences the macrofracture behaviors. These two models have relatively complex geometries and loading conditions and are suitable to show whether the underlying structure of the micropore would have any impacts on the macrofracture behavior.

6.1. Case Study I: Single-edge notched shear test

As discussed above, the material parameters of the single-edge notched shear model are obtained from different MD simulations of a-SiO_2 with different pore shapes as

summarized in Table 2. The mesh discretization (L=0.0017 mm), boundary conditions, and loading conditions are the same for all models as discussed in Section 2.3. Specifically, each model has 24,630 quadrilateral elements with the average element size along the fracture path equal to 0.0017 mm. A prescribed displacement of 0.002 mm increment is applied to each case. The reaction force-displacement for each model is shown in Figure 10, while Figure 11 shows the fracture propagation path for each case at displacement values of 0.45×10^{-3} mm, 0.55×10^{-3} mm, 0.75×10^{-3} mm, and 0.85×10^{-3} mm, respectively.

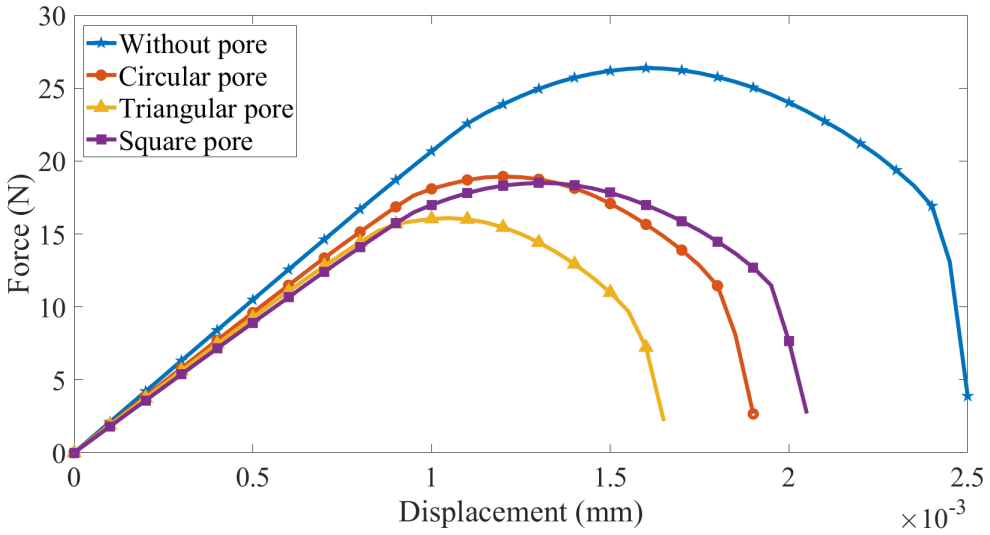

Figure 10: Comparison of displacement vs force for four different samples.

The force-displacement curves in Figure 10 clearly shows the differences among each model. In another word, one can see not only the influence of the porosity (first-order parameter) but also the influence of pore shape (higher-order parameter) on the overall load-displacement curve. The case without a micropore has zero porosity, therefore, it has the largest critical strength and highest stiffness. In the cases with circular, triangular, and square pores, the critical strength and stiffness reduce gradually, even though they have the same porosity. These results were expected as they follow a similar trend observed in the material properties presented in Table 2, where the case without micropore has the highest energy release rate, while cases with circular and square pores have similar energy release rate values, followed by the triangular pore with the lowest value of energy release rate. Thus, as it can be seen from Figure 10, the fracture initiates first in the triangular case as it has the lowest critical energy release rate. A similar trend can be found in terms of the time to failure. However, it is noteworthy that the case

with square pore has a similar energy release rate but relatively lower stiffness compared to the case with circular pore, therefore, its failure occurs at a later time compared to the circular case. Essentially, the material with higher stiffness and strength consumes more energy for the fracture to propagate. It is also worth mentioning that at the failure point in each case, the reaction force drops sharply as shown in Figure 10.

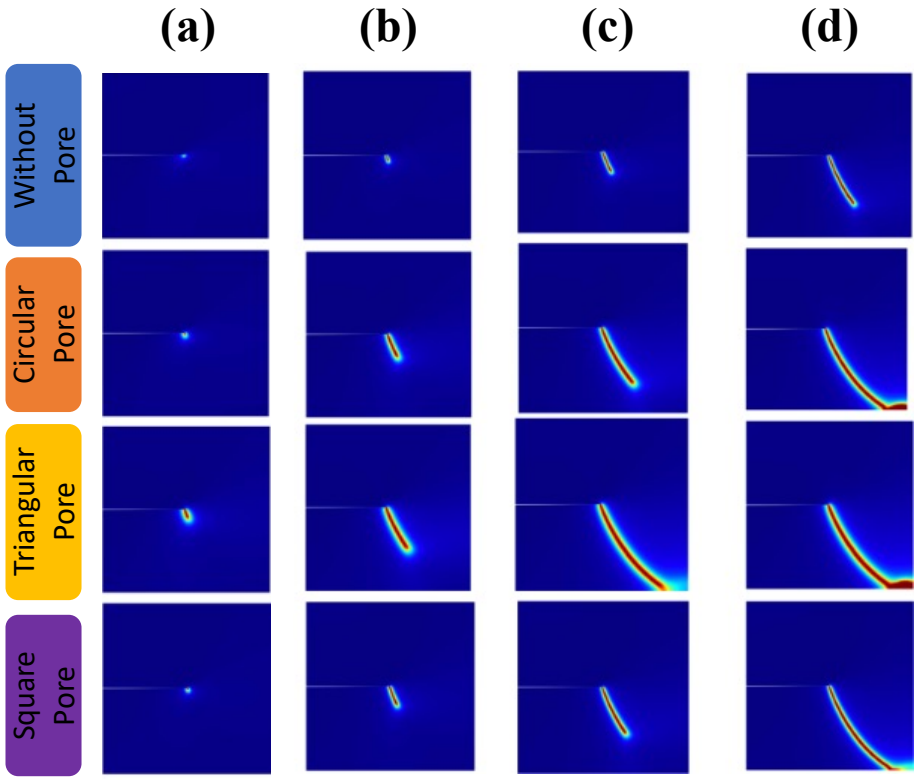

Figure 11: Crack pattern for a-SiO_2 for different pore morphologies at different displacement values (u):
(a) u=0.45e^{-3} mm, (b) u=0.55e^{-3} mm, (c) u=0.75^{-3} mm, (d) u=0.85e^{-3} mm,.

From Figure 11, one can see that there are no significant differences in terms of the crack paths among the four cases. However, the crack is different at prescribed displacements of 0.45×10^{-3} mm, 0.55×10^{-3} mm, 0.75×10^{-3} mm, and $0.85 \times 10^{-}3$ mm. In the triangular case, the crack initiates sooner than any other cases. It also propagates much faster than other cases leading to a much sooner failure. Moreover, the crack width, in this case, is also wider than in other cases. This behavior was expected as the triangular pore has the lowest Young's modulus, energy release rate, and critical tensile strength but highest length scale among all

other cases. Although circular and square cases have similar Young's modulus and energy release rates, the square case has higher tensile strength and lower length scale. Therefore, fracture in circular case propagates faster with a relatively wider crack width compared to the square case. As anticipated, the case without pore has the slowest propagation with the narrowest crack zone.

This example illustrates that the variations of underlying pore structure in porous media will lead to different fracture responses, and the effect of micropore structure can be transmitted to the PF models by integrating the macroscopic material properties evaluated based on MD simulations.

6.2. Case Study II: notched rectangular with three openings

This fracture example has been selected as it has been shown by other researchers [61] that the fracture path is sensitive to the distance of the holes from the initial crack. However, we suspect that the fracture response is also sensitive to the underlying porous structure. The geometry, loading and boundary conditions, and discretization are discussed in section 2.3. The material properties used in this example are listed in Table 1. As the fracture path is a major concern for this example, we primarily focus on the variation of fracture path in each case (i.e., without pore, circular, square, and triangular pore). Figure 12 shows the load-displacement curve associated with each case, while Figure 13 highlights the crack path corresponding to two distinct points of max fracture strength and ultimate failure for each case.

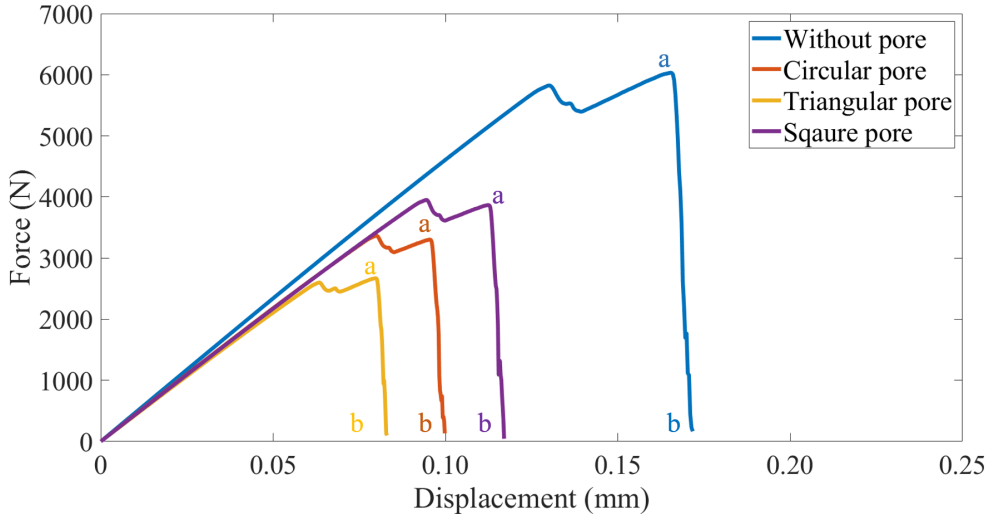

Figure 12: Displacement vs force in four cases.

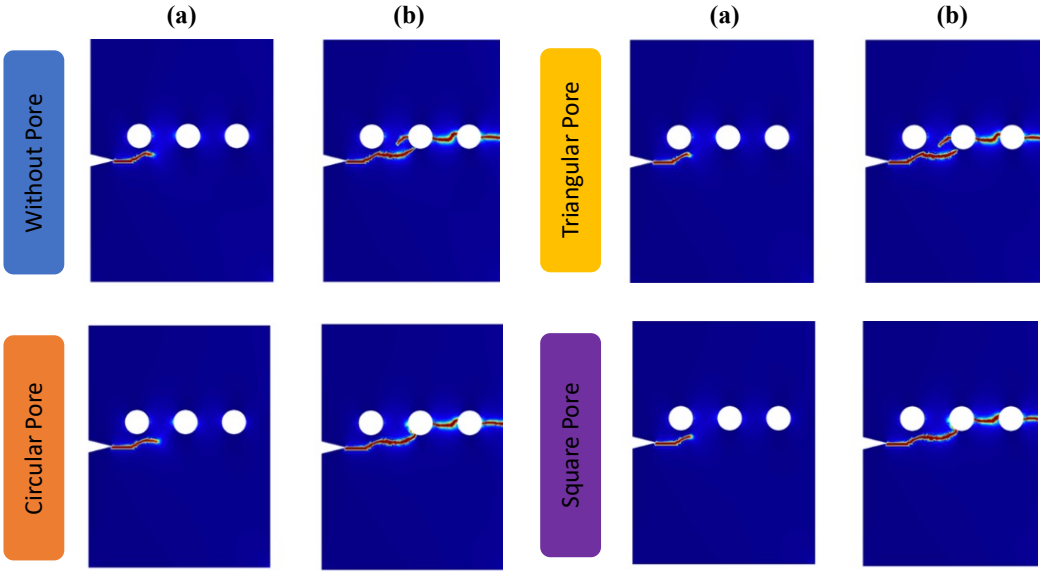

Figure 13: Crack path in the a-SiO_2 model for cases without pore, with circular pore, with square pore, and with triangular pores at points (a) and (b) shown in Figure 12.

Similar to the case study I, the clear differences (e.g., stiffness, max fracture strength, propagation speed, etc.) between each load-displacement curve can be explained based on the differences in material properties derived from the MD simulations. In this case study, we would like to focus on the crack pattern for each pore structure as shown in Figure 12. We primarily compare the fracture pattern at the point of max fracture strength and ultimate failure. These two points correspond to point (a) and (b) shown in Figure 12. Figure 13 shows the fracture path along these points for different pore structures.

From the displacement-reaction force shown in Figure 12, one can see a similar pattern among all cases. This similarity further translates to the overall crack pattern in each case as shown in Figure 13. However, a careful comparison of these plots shows that the fracture pattern varies among all four cases. For example, after the fracture initiates, there is a drop in the peak force values followed by an increase in the reaction force. A closer look in Figure 13 shows that although this trend is similar among all cases, the magnitude and corresponding displacement at which the crack initiates varies in each case. Specifically, cases with circular and square pore show a slightly smooth fracture path, while cases without pore and with triangular pore show a sharp-curved fracture path.

Furthermore, the difference from point (a) to (b) in Figure 12 also indicates that

the fracture path varies among all four cases. As shown in Figure 13, one can see that in cases without pore and with triangular pore, secondary crack initiates on the left side of the middle circle which does not appear in the cases with circular and square pore structures. Overall, such differences in crack initiation and propagation are due to the variation in the underlying morphology that has been captured through MD simulations.

6.3. Results and Discussions

The application of micromechanics in porous media has significantly advanced our understanding of the connection between material properties and the micropore structure [15, 81, 40]. However, we are still facing some challenges to upgrade certain material properties such as energy release rate from the microscale. Particularly, the proper quantities describing the micropore morphology on material behaviors (e.g., fracture) are not available. ReaxFF has been proven to be one of the best force fields with the ability not only to capture the chemical reactions but also to predict the mechanical properties of materials. [21, 84, 11]. ReaxFF also enables us to capture the fluid-solid interaction or chemical reaction within the porous network. Therefore, in this study, for the first time, we explored its potential in predicting macrofracture behavior of porous materials with variations in their micropore structure. We applied the MD-based characterization to the cases containing micropores, and implemented a combined MD and PF framework to investigate the effect of underlying micropore shape in the macrofracture in the porous material.

In porous media, as the first-order factor, porosity remains the dominant parameter in dictating the material properties, but the influence of the higher-order parameters cannot be ignored in engineering and scientific applications [15, 33]. Our numerical case studies highlighted that the pore shape would indeed influence the fracture behaviors (e.g., fracture strength, propagation speed, crack surface, crack growth path) as discussed above. Moreover, the extent of these effects varies based on the macroscopic boundary value problem. For example, in the notched rectangular specimen with three openings, we can see that the fracture pattern varies among all four cases. However, the same influence is not observed in the single-edge notched shear test. Although the porosity plays an influential role in porous materials [33], the pore shape effect is not negligible as it may change the crack path in an unexpected approach. Therefore, it is important to understand the effect of the structure of micropore on the macro behavior of porous materials, particularly in the design of nano material or metamaterials.

Due to the lack of proper quantities to directly upgrade the pore shape effect, in our investigation, we use the material property to indirectly incarnate the pore

shape effect on the macrofracture behaviors. However, we suspect that there may be some information that cannot be transmitted, for example, the tensile strength (the max stress before failure in the tensile test). In our study, the tensile strength values were obtained from the literature and are proportioned based on the ultimate strain ratio of each MD sample. In this estimation, the pore effect may not have been comprehensively considered due to the difference between experimental and theoretical values. Our MD-based tensile strength values are higher than the experimental value which could be due to the fact that defects in materials were not considered in our MD simulations [11]. Finding an appropriate approach to upgrade the tensile strength from the MD simulations to macroscopic continuum simulation is still a challenging task. In the absence of such information, the pore effect may not be completely upgraded from microscale to the macroscale in the combined MD-PF framework. However, the investigation of two examples in this study indicates that the pore effect can be considered in the extended MD-PF framework, although more rigorous studies are still needed.

It should be noted that the critical length scale is an important parameter in PF fracture modeling [53, 68, 30] as it represents the diffusive size of the fracture path and corresponds to the broken zone in the material. In MD simulations, the critical length scale corresponds to the molecular transition zone or the zone with broken bonds [30, 68]. Thus, Patil, et al. [68] and Hasnsen-Dorr, et al [30] proposed to determine the critical length scale from MD simulations. However, one precondition for this method is that the PF model should be comparable to the MD model in terms of domain size, geometry, loading patterns, etc. If the fracture model is too complex, this modeling approach would not be realistic. In our study, we adopted the method proposed in [92], where the length scale is estimated purely based on the macroscopic material properties. As the characterization of materiel properties already consider the microscopic structure, we postulate that the derivation of the critical length scale from the material properties at the macroscale is more suitable for the combined MD-PF method. However, quantitative studies may be still needed to verify this assumption but it is beyond the scope of this study.

7. Conclusion

Considering that the structure of micropore affects the mechanical behavior of porous media [84], in this study, we explored the role of micropore morphology on the macrofracture behaviors in a porous material. To achieve this goal, we extended the combined MD-PF framework to account for micropore structures at the atomic scale using state-of-the-art ReaxFF. Together with a critical length scale based on the macroscopic material properties, this extension allowed us to

investigate the role of micropore morphology on the macrofracture behavior.

Two fracture problems used by the PF fracture community were adopted to investigate the role of different micropores on the macrofracture behavior. In each problem, we looked at four micropore structures: without pore, with circular, triangular, and square pores. MD simulations was performed at the microscale and properties were extracted to be used in the macro PF models. The result of these two examples demonstrated that, although it is commonly known that the porosity has a substantial influence on the macro fracture behaviors of porous media [33, 19], micropore shape also affects the fracture response. Specifically, among the four different pore shapes, fracture in the triangular case initiates and reaches the failure sooner than other cases, although triangular has the same porosity as the circular and square cases. This trend is observed in both single-edge notched shear and rectangular notched with three openings problems. Furthermore, in the notched rectangular with three openings problem, we found that the micropore shape influences the crack pattern as well. For example, in the case of a triangular pore, the fracture path at the points of max reaction force and ultimate failure is different from the fracture path of the circular and square pore. The same trend is not observed in the single-edge notched shear problem. This difference indicates that the extent of micropore effect varies depending on the fracture problems.

These findings enhance our understanding of the correlation between the structure of micropore and the macrofracture behaviors in porous media and demonstrate the importance of considering the micropore shapes in material design and manufacturing. Specifically, such knowledge can assist us to create materials with controllable micropore structures to achieve desirable macroscopic behavior.

This work is based on our previous study [84], where we noticed that for given porosity, the pore orientation is not influential factor to the material properties. That is saying the orientating effects of pore and load is negligible for given porosity. As a result, the pore orientation is not considered. However, the pore orientation may play an important role for mixed pore network. Investigating this effect will be our future research direction. The future work will also focus on the validation of the fracture response in porous media evaluated by the combined MD and PF modeling framework.

Acknowledgement

In this work, the molecular dynamic analysis was supported as part of the Multi-Scale Fluid-Solid Interactions in Architected and Natural Materials (MUSE) Project, an Energy Frontier Research Center funded by the U.S. Department of Energy,

Office of Science, Basic Energy Sciences under Award #DE-SC0019285. The remaining part of the work was supported by Dr. Newell's startup through the University of Utah. This research used resources of the National Energy Research Scientific Computing Center, a DOE Office of Science User Facility supported by the Office of Science of the U.S. Department of Energy under Contract No. DE-AC02-05CH11231. The authors would like to thank the University of Utah Center for High Performance Computing (CHPC) for providing additional computational resources.

Contribution

Bang He: Conceptualization, Software, Validation, Investigation, Writing-Original Draft and Editing. **Truong Vo**: Software, Validation, Writing-Reviewing and Editing. **Pania Newell**: Conceptualization, Supervision, Funding acquisition, Writing-Reviewing and Editing.

References

[1] Abali, B.E., Klunker, A., Barchiesi, E., Placidi, L., 2021. A novel phase-field approach to brittle damage mechanics of gradient metamaterials combining action formalism and history variable. ZAMM - Journal of Applied Mathematics and Mechanics / Zeitschrift für Angewandte Mathematik und Mechanik 101, e202000289. doi:https://doi.org/10.1002/zamm.202000289.

[2] Agathos, K., Ventura, G., Chatzi, E., Bordas, S.P.A., 2018. Stable 3d xfem/vector level sets for non-planar 3d crack propagation and comparison of enrichment schemes. International Journal for Numerical Methods in Engineering 113, 252–276. doi:https://doi.org/10.1002/nme.5611.

[3] Ambati, M., Gerasimov, T., De Lorenzis, L., 2014. A review on phase-field models of brittle fracture and a new fast hybrid formulation. Computational Mechanics 55. doi:10.1007/s00466-014-1109-y.

[4] Belytschko, T., Black, T., 1999. Elastic crack growth in finite elements with minimal remeshing. International Journal for Numerical Methods in Engineering 45, 601–620.

[5] Bharali, R., 2021. Computational homogenisation and solution strategies for phase-field fracture .

[6] Borden, M.J., Verhoosel, C.V., Scott, M.A., Hughes, T.J., Landis, C.M., 2012. A phase-field description of dynamic brittle fracture. Computer Methods in Applied Mechanics and Engineering 217-220, 77–95.

[7] Borst, R., Réthoré, J., Abellan, M.A., 2006. A numerical approach for arbitrary cracks in a fluid-saturated medium. Archive of Applied Mechanics 75, 595–606.

[8] Bourdin, B., Francfort, G., Marigo, J., 2008. The variational approach to fracture. Journal of Elasticity 91, 5–148.

[9] Brezzi, F., Fortin, M., 1991. Mixed and Hybrid Finite Element Methods. Springer-Verlag, Berlin, Heidelberg.

[10] Brochard, L., Hantal, G., Laubie, H., Ulm, F.J., Pellenq, R.J.M., . Fracture Mechanisms in Organic-Rich Shales: Role of Kerogen. pp. 2471–2480. doi:10.1061/9780784412992.288.

[11] Chakraborty, P., Zhang, Y., Tonks, M.R., 2016. Multi-scale modeling of microstructure dependent intergranular brittle fracture using a quantitative phase-field based method. Computational Materials Science 113, 38–52.

[12] Chowdhury, S., (Gama) Haque, B., Gillespie Jr, J., 2016. Molecular dynamics simulations of the structure and mechanical properties of silica glass using reaxff. Journal of Materials Science 51. doi:10.1007/s10853-016-0242-8.

[13] Chowdhury, S.C., Wise, E.A., Ganesh, R., Gillespie Jr, J.W., 2019. Effects of surface crack on the mechanical properties of Silica: A molecular dynamics simulation study. Engineering Fracture Mechanics 207, 99–108.

[14] Cottrell, J.A., Hughes, T.J.R., Bazilevs, Y., 2009. Isogeometric Analysis: Toward Integration of CAD and FEA. 1st ed., Wiley Publishing.

[15] Coussy, O., 2005. Poromechanics. John Wiley & Sons, Ltd, Chichester, UK.

[16] Cramer, M., Sevostianov, I., 2009. Effect of pore distribution on elastic stiffness and fracture toughness of porous materials. International Journal of Fracture 160, 189–196. doi:10.1007/s10704-009-9416-6.

[17] Crawford, J., 1994. The relationship between structure and the hydraulic conductivity of soil. European Journal of Soil Science 45, 493–502.

[18] De Borst, R., 2018. Chapter 1 - introduction, in: De Borst, R. (Ed.), Computational Methods for Fracture in Porous Media. Elsevier, pp. 1–12.

[19] De Borst, R., Verhoosel, V., 2016. Gradient damage vs phase-field approaches for fracture: similarities and differences. Computer Methods in Applied Mechanics and Engineering 312, 78–94.

[20] D'Orazio, M., Lenci, S., Graziani, L., 2014. Relationship between fracture toughness and porosity of clay brick panels used in ventilated façades: initial investigation. Engineering Fracture Mechanics 116, 108–121.

[21] Du, T., Blum, M., Chen, C., Muraleedharan, M.G., van Duin, A.C., Newell, P., 2021. Nanomechanical investigation of the interplay between pore morphology and crack orientation of amorphous silica. Engineering Fracture Mechanics 250, 107749.

[22] Dutta, T., Tarafdar, S., 2003. Fractal pore structure of sedimentary rocks: Simulation by ballistic deposition. Journal of Geophysical Research: Solid Earth 108.

[23] Egger, A., Pillai, U., Agathos, K., Kakouris, E., Chatzi, E., Aschroft, I.A., Triantafyllou, S.P., 2019. Discrete and Phase Field Methods for Linear Elastic Fracture Mechanics: A Comparative Study and State-of-the-Art Review. Applied Sciences 9, 2436.

[24] Ehlers, W., Luo, C., 2017. A phase-field approach embedded in the theory of porous media for the description of dynamic hydraulic fracturing. Computer Methods in Applied Mechanics and Engineering 315, 348–368. doi:https://doi.org/10.1016/j.cma.2016.10.045.

[25] Fan, H.B., Wong, C.K.Y., Yuen, M.M.F., 2006. Prediction of material properties of epoxy materials using molecular dynamic simulation, in: EuroSime 2006 - 7th International Conference on Thermal, Mechanical and Multiphysics Simulation and Experiments in Micro-Electronics and Micro-Systems, pp. 1–4. doi:10.1109/ESIME.2006.1644033.

[26] Fogarty, J.C., Aktulga, H.M., Grama, A.Y., Van Duin, A.C., Pandit, S.A., 2010. A reactive molecular dynamics simulation of the silica-water interface. The Journal of chemical physics 132, 174704.

[27] Griffith, A.A., VI., G.I.T., 1921. The phenomena of rupture and flow in solids. Philosophical Transactions of the Royal Society of London. Series A 221, 163–198.

[28] Grøva, M., 2012. Two-Phase Flow in Porous Media: Scaling of Steady-State Effective Permeability. Journal of Physics: Conference Series 319.

[29] Gupta, P., Duarte, C.A., 2014. Simulation of non-planar three-dimensional hydraulic fracture propagation. International Journal for Numerical and Analytical Methods in Geomechanics 38, 1397–1430.

[30] Hansen-Dörr, A.C., Wilkens, L., Croy, A., Dianat, A., Cuniberti, G., Kästner, M., 2019. Combined molecular dynamics and phase-field modelling of crack propagation in defective graphene. Computational Materials Science 163, 117 – 126. doi:https://doi.org/10.1016/j.commatsci.2019.03.028.

[31] Hao, T., Hossain, Z.M., 2019. Atomistic mechanisms of crack nucleation and propagation in amorphous silica. Physical Review B 100, 014204.

[32] He, B., Newell, P., 2018. A Numerical Scheme to Model Two-Phase Flow-Driven Fracture in Subsurface Geological Material, in: American Rock Mechanics Association 2018, Seattle, WA.

[33] He, B., Schuler, L., Newell, P., 2020. A numerical-homogenization based phase-field fracture modeling of linear elastic heterogeneous porous media. Computational Materials Science 176, 109519.

[34] Heider, Y., Markert, B., 2017. A phase-field modeling approach of hydraulic fracture in saturated porous media. Mechanics Research Communications 80, 38–46.

[35] Hirshikesh, Jansari, C., Kannan, K., Annabattula, R., Natarajan, S., 2019. Adaptive phase field method for quasi-static brittle fracture using a recovery based error indicator and quadtree decomposition. Engineering Fracture Mechanics 220, 106599.

[36] Hunt, A.G., Sahimi, M., 2017. Flow, transport, and reaction in porous media: Percolation scaling, critical-path analysis, and effective medium approximation. Reviews of Geophysics 55, 993–1078.

[37] Jelitto, H., Schneider, G., 2018. A geometric model for the fracture toughness of porous materials. Acta Materialia 151, 443–453.

[38] Jeong, H., Signetti, S., Han, T.S., Ryu, S., 2018. Phase field modeling of crack propagation under combined shear and tensile loading with hybrid formulation. Computational Materials Science 155, 483 – 492.

[39] Jo, H.S., Lee, G.W., 2017. Investigation of mechanical and thermal properties of silica-reinforced epoxy composites by using experiment and empirical model. Materials Today: Proceedings 4, 6178–6187. doi:https://doi.org/10.1016/j.matpr.2017.06.113.

[40] Kachanov, M., Sevostianov, I., 2005. On quantitative characterization of microstructures and effective properties. International Journal of Solids and Structures 42, 309–336. Micromechanics of Materials.

[41] Krishnamoorthy, A., Rajak, P., Norouzzadeh, P., Singh, D.J., Kalia, R.K., Nakano, A., Vashishta, P., 2019. Thermal conductivity of mos2 monolayers from molecular dynamics simulations. AIP Advances 9, 035042. doi:10.1063/1.5085336.

[42] Kubik, J., 1988. Macro description of micro pore structure in regard to fluid flow through porous media, in: Unger, K., Rouquerol, J., Sing, K., Kral, H. (Eds.), Characterization of Porous Solids. Elsevier. volume 39 of *Studies in Surface Science and Catalysis*, pp. 345–353.

[43] Laubie, H., Monfared, S., Radjaï, F., Pellenq, R., Ulm, F.J., 2017. Disorder-induced stiffness degradation of highly disordered porous materials. Journal of the Mechanics and Physics of Solids 106, 207–228.

[44] Leguillon, D., Piat, R., 2008. Fracture of porous materials – Influence of the pore size. Engineering Fracture Mechanics 75, 1840–1853.

[45] Li, J., Lu, B., Zhou, H., Tian, C., Xian, Y., Hu, G., Xia, R., 2019. Molecular dynamics simulation of mechanical properties of nanocrystalline platinum: Grain-size and temperature effects. Physics Letters A 383, 1922–1928.

[46] Liu, P., Chen, G., 2014. Porous materials: Processing and applications. Porous Materials: Processing and Applications , 1–560.

[47] Loew, P.J., Peters, B., Beex, L.A., 2020a. Fatigue phase-field damage modeling of rubber using viscous dissipation: Crack nucleation and propagation. Mechanics of Materials 142, 103282.

[48] Loew, P.J., Poh, L.H., Peters, B., Beex, L.A., 2020b. Accelerating fatigue simulations of a phase-field damage model for rubber. Computer Methods in Applied Mechanics and Engineering 370, 113247.

[49] Lu, X., Viljanen, M., 2011. 10 - Fibrous insulation materials in building engineering applications, in: Fangueiro, R. (Ed.), Fibrous and Composite Materials for Civil Engineering Applications. Woodhead Publishing. Woodhead Publishing Series in Textiles, pp. 271–305.

[50] Markicevic, B., Djilali, N., 2006. Two-scale modeling in porous media: relative permeability predictions. Physics of Fluids 18, 33–101.

[51] Martínez-Pañeda, E., Golahmar, A., Niordson, C.F., 2018. A phase field formulation for hydrogen assisted cracking. Computer Methods in Applied Mechanics and Engineering 342, 742–761.

[52] Mei, H., Yang, Y., van Duin, A.C., Sinnott, S.B., Mauro, J.C., Liu, L., Fu, Z., 2019. Effects of water on the mechanical properties of silica glass using molecular dynamics. Acta Materialia 178, 36–44.

[53] Miehe, C., Hofacker, M., Welschinger, F., 2010a. A phase field model for rate-independent crack propagation: robust algorithmic implementation based on operator splits. Computer Methods in Applied Mechanics and Engineering 199, 2765–2778.

[54] Miehe, C., Mauthe, S., 2016. Phase field modeling of fracture in multi-physics problems. Part III. Crack driving forces in hydro-poro-elasticity and hydraulic fracturing of fluid-saturated porous media. Computer Methods in Applied Mechanics and Engineering 304, 619–655.

[55] Miehe, C., Welschinger, F., Hofacker, M., 2010b. Thermodynamically consistent phase-field models of fracture: variational principles and multi-field fe implementations 83, 1273–1311.

[56] Mikelic, A., Wheeler, F., Wick, T., 2015. A phase-field method for propagating fluid-filled fractures coupled to a surrounding porous medium. SIAM Multiscale Modeling and Simulation 13, 367–398.

[57] MikelicÂ, A., Wheeler, F., Wick, T., 2015. A phase-field method for propagating fluid-filled fractures coupled to a surrounding porous medium, in: SIAM Multiscale Modeling and Simulation, p. 367â398.

[58] Moës, N., Dolbow, J., Belytschko, T., 1999. A finite element method for crack growth without remeshing. International Journal for Numerical Methods in Engineering 46, 131–150.

[59] Mohammadnejad, T., Khoei, A.R., 2013. Hydro-mechanical modeling of cohesive crack propagation in multiphase porous media using the extended finite element method. International Journal for Numerical and Analytical Methods in Geomechanics 37, 1247–1279.

[60] Molnár, G., Gravouil, A., 2017. 2D and 3D Abaqus implementation of a robust staggered phase-field solution for modeling brittle fracture. Finite Elements in Analysis and Design 130, 27–38.

[61] Msekh, M.A., Sargado, J.M., Jamshidian, M., Areias, P.M., Rabczuk, T., 2015. Abaqus implementation of phase-field model for brittle fracture. Computational Materials Science 96, 472–484. Special Issue Polymeric Composites.

[62] Munetoh, S., Motooka, T., Moriguchi, K., Shintani, A., 2007. Interatomic potential for Si–O systems using Tersoff parameterization. Computational Materials Science 39, 334–339.

[63] Navidtehrani, Y., Betegón, C., Martínez-Pañeda, E., 2021. A unified abaqus implementation of the phase field fracture method using only a user material subroutine. Materials 14. doi:10.3390/ma14081913.

[64] Nguyen, V.P., Kerfriden, P., Bordas, S.P., 2014. Two- and three-dimensional isogeometric cohesive elements for composite delamination analysis. Composites Part B: Engineering 60, 193–212. doi:https://doi.org/10.1016/j.compositesb.2013.12.018.

[65] Nielsen, L.F., 1990. Strength and stiffness of porous materials. Journal of the American Ceramic Society 73, 2684–2689.

[66] Ozaki, S., Aoki, Y., Osada, T., Takeo, K., Nakao, W., 2018. Finite element analysis of fracture statistics of ceramics: Effects of grain size and pore size distributions. Journal of the American Ceramic Society 101, 3191–3204.

[67] Padilla, C.A.H., Patil, S.P., Heider, Y., Markert, B., 2017. 3d modeling of brittle fracture using a joint all-atom and phase-field approach. GAMM-Mitteilungen 40, 91–101. doi:https://doi.org/10.1002/gamm.201720002.

[68] Patil, S.P., Heider, Y., Padilla, C.A.H., Cruz-Chú, E.R., Markert, B., 2016. A comparative molecular dynamics-phase-field modeling approach to brittle fracture. Computer Methods in Applied Mechanics and Engineering 312, 117 – 129.

[69] Pedone, A., Malavasi, G., Menziani, M.C., Cormack, A.N., Segre, U., 2006. A new self-consistent empirical interatomic potential model for oxides, silicates, and silica-based glasses. The Journal of Physical Chemistry B 110, 11780–11795.

[70] Peerlings, R.H.J., De Borst, R., Brekelmans, W.A.M., Geers, M.G.D., 1998. Gradient-enhanced damage modelling of concrete fracture. Mechanics of Cohesive-frictional Materials 3, 323–342.

[71] Plimpton, S., 1995. Fast parallel algorithms for short-range molecular dynamics. Journal of computational physics 117, 1–19.

[72] Rimsza, J., Deng, L., Du, J., 2016. Molecular dynamics simulations of nanoporous organosilicate glasses using reactive force field (reaxff). Journal of Non-Crystalline Solids 431, 103–111. doi:https://doi.org/10.1016/j.jnoncrysol.2015.04.031. iSNOG 2014.

[73] Rimsza, J.M., Jones, R.E., Criscenti, L.J., 2018. Crack propagation in silica from reactive classical molecular dynamics simulations. Journal of the American Ceramic Society 101, 1488–1499.

[74] Satake, K., Okada, K., Muramatsu, M., 2021. Phase-field crack analysis using estimated transition zone of crack by molecular dynamics simulation. AIP Advances 11, 065206.

[75] Stillinger, F.H., Weber, T.A., 1985. Computer simulation of local order in condensed phases of silicon. Physical review B 31, 5262.

[76] Su, B.L., Sanchez, C., Yang, X.Y., 2012. Hierarchically Structured Porous Materials : From Nanoscience to Catalysis, Separation, Optics, Energy, and Life Science. Wiley-VCH.

[77] Suh, H.S., Sun, W., 2021. Asynchronous phase field fracture model for porous media with thermally non-equilibrated constituents. Computer Methods in Applied Mechanics and Engineering 387, 114182. doi:https://doi.org/10.1016/j.cma.2021.114182.

[78] Sutula, D., Kerfriden, P., van Dam, T., Bordas, S.P., 2018. Minimum energy multiple crack propagation. Part III: XFEM computer implementation and applications. Engineering Fracture Mechanics 191, 257–276.

[79] Torres-Sanchez, C., McLaughlin, J., Bonallo, R., 2018. Effect of pore size, morphology and orientation on the bulk stiffness of a porous Ti35Nb4Sn alloy. Journal of Materials Engineering and Performance 27, 2899–2909.

[80] Tsai, D.H., 1979. The virial theorem and stress calculation in molecular dynamics. The Journal of Chemical Physics 70, 1375–1382. doi:10.1063/1.437577.

[81] Tsukrov, I., Kachanov, M., 2000. Effective moduli of an anisotropic material with elliptical holes of arbitrary orientational distribution. International Journal of Solids and Structures 37, 5919–5941.

[82] Van Beest, B., Kramer, G.J., Van Santen, R., 1990. Force fields for silicas and aluminophosphates based on ab initio calculations. Physical Review Letters 64, 1955.

[83] Vazic, B., Abali, B.E., Yang, H., Newell, P., 2021. Mechanical analysis of heterogeneous materials with higher-order parameters. Engineering with Computers .

[84] Vo, T., He, B., Blum, M., Damone, A., Newell, P., 2020. Molecular scale insight of pore morphology relation with mechanical properties of amorphous silica using reaxff. Computational Materials Science 183, 109881. doi:https://doi.org/10.1016/j.commatsci.2020.109881.

[85] Wang, X., Han, D., Hong, Y., Sun, H., Zhang, J., Zhang, J., 2019. Machine learning enabled prediction of mechanical properties of Tungsten Disulfide Monolayer. ACS Omega 4, 10121–10128.

[86] Wilson, Z.A., Landis, C.M., 2016. Phase-field modeling of hydraulic fracture. Journal of the Mechanics and Physics of Solids 96, 264–290.

[87] Wu, J.Y., Nguyen, V.P., Thanh Nguyen, C., Sutula, D., Bordas, S., Sinaie, S., 2019. Phase field modelling of fracture. Advances in Applied Mechanics 53.

[88] Yoshioka, K., Bourdin, B., 2016. A variational hydraulic fracturing model coupled to a reservoir simulator. International Journal of Rock Mechanics and Mining Sciences 88, 137–150.

[89] Zdravkov, B.D.and Cermák, J., ˇSefara, M., Janků, J., 2007. Pore classification in the characterization of porous materials: a perspective. Central European Journal of Chemistry 5, 385–395.

[90] Zhang, H., Ge, X., Ye, H., 2006. Effective thermal conductivity of two-scale porous media. Applied Physics Letters 89.

[91] Zhang, X., Sloan, W., Vignes, C., Sheng, D., 2017a. A modifcation of the phase-feld model for mixed mode crack propagation in rock-like materials. Comput. Methods Appl. Mech. Engrg. 322, 123â136.

[92] Zhang, X., Vignes, C., Sloan, S., Sheng, D., 2017b. Numerical evaluation of the phase-field model for brittle fracture with emphasis on the length scale. Computational Mechanics 59. doi:10.1007/s00466-017-1373-8.

[93] Zhang, Y.Y., Pei, Q.X., Sha, Z.D., Zhang, Y.W., 2019. A molecular dynamics study of the mechanical properties of h-BCN monolayer using a modified Tersoff interatomic potential. Physics Letters A 383, 2821 – 2827. doi:https://doi.org/10.1016/j.physleta.2019.05.055.

[94] Zhou, S., Zhuang, X., Rabczuk, T., 2018a. A phase-field modeling approach of fracture propagation in poroelastic media. Engineering Geology 240, 189–203.

[95] Zhou, S., Zhuang, X., Zhu, H., Rabczuk, T., 2018b. Phase field modelling of crack propagation, branching and coalescence in rocks. Theoretical and Applied Fracture Mechanics 96, 174–192.